Manipulation and Generation of Supercurrent in Out-of-Equilibrium Josephson Tunnel Nanojunctions

S. Tirelli,[1] A. M. Savin,[2] C. Pascual Garcia,[1] J. P. Pekola,[2] F. Beltram,[1] and F. Giazotto[1,*]

[1]*NEST CNR-INFM and Scuola Normale Superiore, I-56126 Pisa, Italy*

[2]*Low Temperature Laboratory, Helsinki University of Technology, P.O. Box 3500, FIN-02015 TKK, Finland*

(Received 16 April 2008; published 14 August 2008)

We demonstrate experimentally the manipulation of supercurrent in Al-AlO_x-Ti Josephson tunnel junctions by injecting quasiparticles in a Ti island from two additional tunnel-coupled Al superconducting reservoirs. Both supercurrent enhancement and quenching with respect to equilibrium are achieved. We demonstrate cooling of the Ti line by quasiparticle injection from the normal state deep into the superconducting phase. A model based on heat transport and the nonmonotonic current-voltage characteristic of a Josephson junction satisfactorily accounts for our findings.

DOI: 10.1103/PhysRevLett.101.077004 PACS numbers: 74.50.+r, 73.23.−b, 74.78.Na, 85.25.Cp

Nonequilibrium dynamics in superconducting nanocircuits is currently the focus of an intense experimental and theoretical effort [1,2]. In this context, the control of the Josephson current in superconductor-normal metal-superconductor (SNS) weak links is receiving much attention. In these systems supercurrent is manipulated by modifying the quasiparticle energy distribution in the N region via current injection from external terminals [3–5]. There have been some successful demonstrations of such out-of-equilibrium SNS junctions [6–9]. On the other hand, it was predicted [10,11] that supercurrent can be controlled in all-superconducting tunnel structures as well. In this case quasiparticle injection [12–17] leads to intriguing features peculiar to out-of-equilibrium superconductors.

In this Letter we report on control of the Josephson coupling in a small S island by injecting quasiparticles from tunnel-coupled superconducting leads. Both supercurrent enhancement and suppression with respect to equilibrium, as well as generation at temperatures above the island critical temperature were achieved by changing the quasiparticle injection rate. Our findings are explained within a model relating the superconducting state of the island to the heat flux driven through it upon injection.

Figure 1 shows a scanning electron micrograph of a typical structure along with a scheme of the measurement setup. The core of the sample consists of a $SIS'IS$ control line, i.e., a titanium (Ti) superconducting island (S') symmetrically connected at its ends via AlO_x barriers (I) with normal-state resistance R_T each to two aluminum (Al) superconducting reservoirs (S). Two additional Al-AlO_x-Ti probe junctions, with normal-state resistance R_J each and placed in the center of the island, are used to measure the Josephson current (I_J) of their nominally symmetric series connection. Our samples were fabricated by electron beam lithography and two-angle shadow-mask evaporation. The measurements were performed in a dilution refrigerator at subkelvin temperatures measured with a RuO_2 resistor calibrated against Coulomb blockade thermometer [2]. The experiment consists of measuring at different bath temperatures (T_{bath}) the current-voltage characteristic (I_{pr} vs V_{pr}) of the series connection of the central SIS' Josephson junctions while imposing a fixed voltage (V_{inj}) across the lateral Al reservoirs. As we shall show, this will lead to a change in temperature of S' which determines the dynamics of the Josephson junctions.

Figure 2 shows the electrical characterization of two structures, in the following referred to as Sample A (whose essential parameters are $R_T \simeq 1.43$ kΩ, $R_J \simeq 2.8$ kΩ and a 45-nm-thick Ti island of area 250×2550 nm^2), and Sample B (with $R_T \simeq 710$ Ω, $R_J \simeq 1.56$ kΩ and a 40-nm-thick Ti island of area 650×1500 nm^2). The critical temperature (T_c') of the Ti layer is ∼500 mK for sample A and ∼210 mK for sample B. Panels (a) and (b) display the low-temperature I_{pr} vs V_{pr} characteristics of sample A and

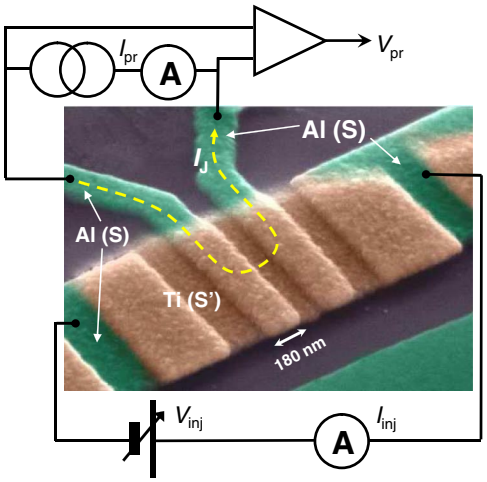

FIG. 1 (color online). A typical structure (sample B) showing a schematic of the measurement setup. In the middle, a Ti superconducting island (S') is connected to four Al electrodes (S) through tunnel junctions. I_J denotes the Josephson current flowing through the two inner Al-AlO_x-Ti tunnel junctions.

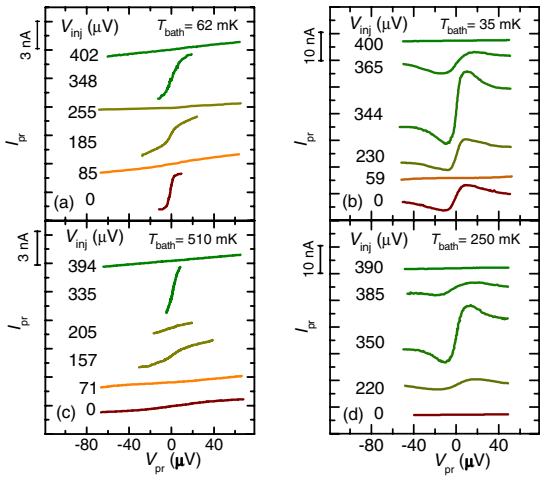

FIG. 2 (color online). I_{pr} vs V_{pr} for various values of V_{inj}: (a) Sample A, $T_{bath} = 62$ mK; (b) sample B, $T_{bath} = 35$ mK; (c) sample A, $T_{bath} = 510$ mK; (d) sample B, $T_{bath} = 250$ mK. The curves are vertically offset for clarity.

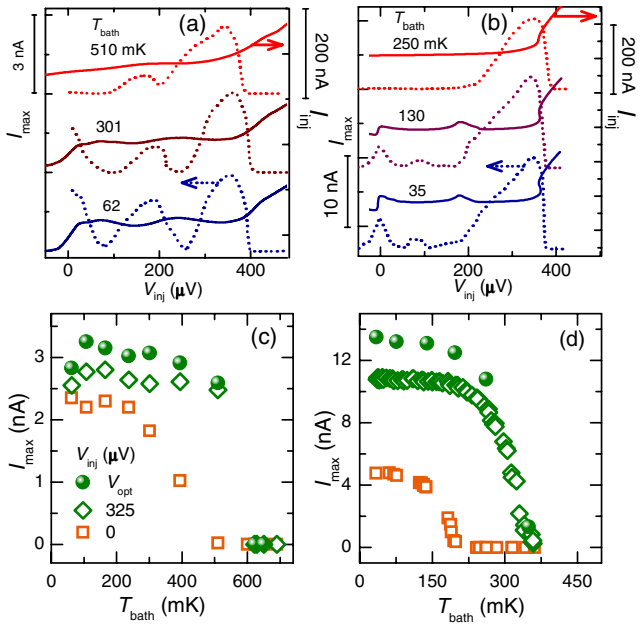

FIG. 3 (color online). (a) Left axis: I_{max} vs V_{inj} at three different T_{bath} for sample A. Right axis: Injector characteristics I_{inj} vs V_{inj} at the same bath temperatures. (b) The same as in (a) for sample B. (c) I_{max} vs T_{bath} for three different values of V_{inj} for sample A. (d) The same as in (c) for sample B.

B, respectively, for several values of the injection voltage V_{inj}. Each characteristic corresponds to a different V_{inj}, and the curves are vertically offset for clarity. In equilibrium, at $V_{inj} = 0$, the supercurrent manifests itself as a peak around zero bias in the current-voltage characteristic. As will be explained with further details, upon increasing the injection voltage the supercurrent behaves nonmonotonically, being initially suppressed, then showing typically two peaks at intermediate injection voltages. Further increase of V_{inj} leads to a monotonic supercurrent decay, and to a complete quenching for $V_{inj} \gtrsim 400$ μV. In Sample B the peak amplitude is enhanced by almost a factor of 3 with respect to equilibrium. The supercurrent response in the high-temperature regime [see panels (c) and (d) for Sample A and B, respectively] is different. In particular, while the equilibrium supercurrent is already vanishing, as T_{bath} exceeds the critical temperature of the Ti island, it is generated by increasing V_{inj} at an injection voltage which cools S' from the normal into the superconducting state. This occurs thanks to hot quasiparticle extraction provided by the Al reservoirs [2,10,11]. By increasing V_{inj} even further leads to another maximum of supercurrent followed by full suppression. Although somewhat different in terms of characteristic parameters, both samples show similar behavior.

The full dependence of the maximum supercurrent I_{max} on V_{inj} at different bath temperatures is displayed on the left axis of Figs. 3(a) and 3(b) for sample A and B, respectively. I_{max} is defined as the average between the amplitudes of positive and negative peaks of I_{pr}. It is a symmetric function of V_{inj} based on electron-hole symmetry, so that just the dependence on positive V_{inj} is shown. As we shall show in the following, the features present at small V_{bias} in the supercurrent response are related to the shape of the current-voltage characteristic of the injectors (I_{inj} vs V_{inj}), shown on the right axis of Figs. 3(a) and 3(b) for the same T_{bath}. In particular, in addition to a current enhancement around $V_{inj} = 0$ originating from Josephson coupling in the lateral SIS' junctions, the curves at lower T_{bath} show a marked peak centered around the middle of the characteristic which disappears as soon as S' undergoes a transition into the normal state.

Figures 3(c) and 3(d) show the I_{max} vs T_{bath} characteristic for sample A and B, respectively, at three different values of I_{inj}. For $V_{inj} = 0$ (open squares) the equilibrium supercurrent saturates at low T_{bath} where it obtains values as high as $\simeq$2.35 nA and $\simeq$4.8 nA for sample A and B, respectively, while it is gradually reduced by increasing the temperature, being completely suppressed at $T_{bath} \simeq$ 500 mK and $\simeq$210 mK, i.e., at the critical temperature of sample A and B, respectively. The low-temperature supercurrent amplitudes are suppressed in both samples by about an order of magnitude as compared to the Ambegaokar-Baratoff theoretical prediction [18]. This is however expected for ultrasmall Josephson tunnel junctions influenced by environment fluctuations [19,20]. For a chosen injection voltage, e.g., at $V_{inj} = 325$ μV, I_{max} saturates at low T_{bath} at $\simeq$2.55 nA for sample A, and $\simeq$10.8 nA for sample B. The maximum supercurrent survives under injection up to $T_{bath} \simeq 630$ mK for sample A and $\simeq$360 mK

for sample B, i.e., well above the equilibrium critical temperature. This means that we can cool the samples by quasiparticle current from the normal into the superconducting state. Also shown is the temperature dependence at the optimized bias voltage ($V_{\rm opt}$) which maximizes $I_{\rm max}$ (solid dots).

Our observations of nonmonotonic dependence of the probe supercurrent on bias voltage and of a peak in the current in the middle of the superconducting gap can both be explained qualitatively within a very simple model. The key observation is that the bias voltage dependence of the current of a single injector junction is nonmonotonic because it can be carried by Cooper pairs (supercurrent around zero voltage) and by quasiparticles (near and above the gap voltage). Then, as a function of bias voltage $V_{\rm inj}$ across the two injecting junctions, the evolution of the voltage across each individual junction is as follows [see the energy-band diagrams in Fig. 4(a)]. At around zero bias, both junctions carry supercurrent, seen as a peak in the current-voltage characteristic. Therefore one of the junctions, i.e., the one with smaller critical current [for instance, left (L) injector in Fig. 4(a)], switches into the quasiparticle branch: the total voltage then equals that across this "weaker" junction, while the other one remains in the approximately zero voltage supercurrent branch. In this situation, when the voltage is approximately $(\Delta_S - \Delta_{S'})/e$ [2,10,11], there is an increase of Josephson critical current of the probe junctions, thanks to enhanced cooling power ($\dot{Q}_L$) due to quasiparticle current in the L junction, i.e., $\dot{Q}_L \neq 0$. Here $\Delta_{S,S'}$ is the BCS energy gap in S (S'). In the middle of the gap region at $(\Delta_S + \Delta_{S'})/e$, one of the junctions reaches the steep onset of quasiparticle current leading to a peak in control current. Above this bias, also the second junction [i.e., right (R) injector in Fig. 4(a)] switches into quasiparticle branch providing finite cooling power, i.e., $\dot{Q}_R \neq 0$. Now the voltage is divided approximately equally across the two junctions, and at intermediate voltages above $(\Delta_S + \Delta_{S'})/e$ cooling power is small until it maximizes at $2(\Delta_S - \Delta_{S'})/e$ [2,10,11] resulting in another maximum in probe supercurrent. The final increase of current $I_{\rm inj}$ in the control junctions occurs at $2(\Delta_S + \Delta_{S'})/e$, where both junctions have an approximately equal voltage corresponding to the onset of quasiparticle current: this results in large current, heating of the S' island, and subsequent quench of the probe supercurrent.

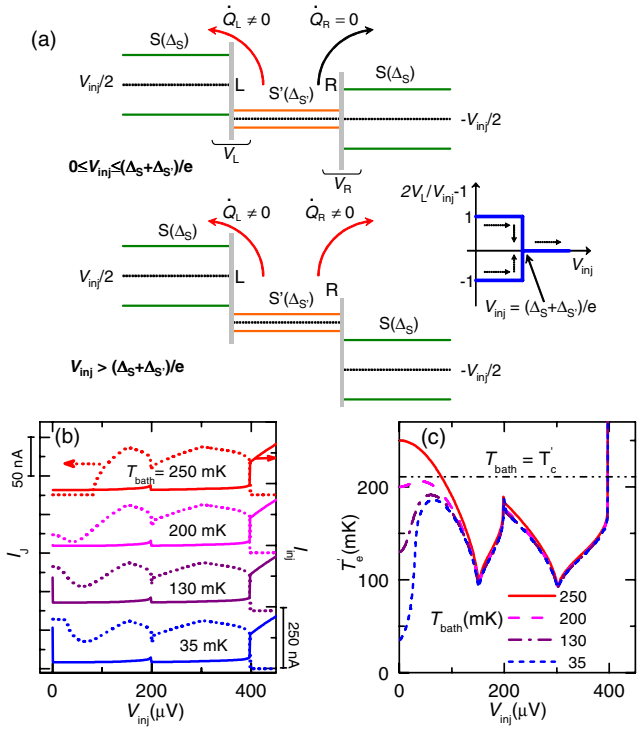

FIG. 4 (color online). (a) Energy-band diagram of the biased $SIS'IS$ control line. Also shown on the right side is the voltage drop V_L across left interface. (b) Left axis: I_J vs $V_{\rm inj}$ calculated for a few values of $T_{\rm bath}$. Right axis: $I_{\rm inj}$ vs $V_{\rm inj}$ calculated for the same $T_{\rm bath}$. The curves are vertically offset for clarity. (c) Calculated T'_e vs $V_{\rm inj}$ for the same $T_{\rm bath}$ as in (b). The horizontal line indicates Ti critical temperature of sample B.

A more quantitative analysis can be carried out as follows. The total electric current flowing through left and right injectors can be written as $I^{L,R}_{\rm inj} = I^{L,R}_J + I^{L,R}_{\rm qp}$, where $I^{L,R}_J \neq 0$ for $V_{L,R} = 0$ is the Ambegaokar-Baratoff critical current of the injectors [18], $V_{L,R}$ is the voltage drop across $L(R)$ interface [see Fig. 4(a)], while $I^{L,R}_{\rm qp} = \pm\frac{1}{eR_T} \times \int d\epsilon \mathcal{N}_S(\tilde{\epsilon}_{L,R})\mathcal{N}_{S'}(\bar{\epsilon})[f_0(\tilde{\epsilon}_{L,R}, T_{\rm bath}) - f_0(\bar{\epsilon}, T'_e)]$ is the quasiparticle current. Here, $\tilde{\epsilon}_{L,R} = \epsilon \mp eV_{\rm inj}/2$, $\bar{\epsilon} = \epsilon - e(V_{\rm inj}/2 - V_L)$, $f_0(\epsilon, T)$ is the Fermi-Dirac function at temperature T, and $\mathcal{N}_{S,S'}(\epsilon)$ is the smeared density of states of $S(S')$. In particular we set $\mathcal{N}_{S,S'}(\epsilon) = |{\rm Re}[(\epsilon + i\Gamma_{S,S'})/\sqrt{(\epsilon + i\Gamma_{S,S'})^2 - \Delta^2_{S,S'}}]|$, where $\Gamma_{S,S'}$ accounts for quasiparticle states within the gap in $S(S')$ [2].

The voltage drop across $L(R)$ interface resulting from biasing with $V_{\rm inj}$ follows from the conservation of the total current, i.e., $I^L_{\rm inj} = I^R_{\rm inj}$ with $V_L + V_R = V_{\rm inj}$. The solution for V_L [shown on the right side of Fig. 4(a)] is $2V_L/V_{\rm inj} - 1 = \pm 1$ for $0 \leq V_{\rm inj} \leq (\Delta_S + \Delta_{S'})/e$, and $V_L = V_{\rm inj}/2$ for $V_{\rm inj} > (\Delta_S + \Delta_{S'})/e$, meaning that only one junction is initially in the dissipative regime [L (R) junction in the upper (lower) branch]. The threshold for equal voltage division is $V_{\rm inj} \simeq (\Delta_S + \Delta_{S'})/e$ and it depends only marginally on the asymmetry between the two injector junctions.

The supercurrent of the probe junctions depends on the quasiparticle distribution in S' under voltage biasing [10,11]. Strong electron-electron interaction drives the electron system in S' into local thermal (quasi)equilibrium described by a Fermi-Dirac function at an electron temperature T'_e which may differ from $T_{\rm bath}$ [2]. The maximum Josephson current flowing through the central SIS' junctions is given by [10,11]

$$I_J = \frac{1}{2eR_J}\left|\int d\epsilon\{[1-2f_0(\epsilon,T'_e)]\mathrm{Re}[\mathcal{F}_{S'}(\epsilon)]\mathrm{Im}[\mathcal{F}_S(\epsilon)] + [1-2f_0(\epsilon,T_{\mathrm{bath}})]\mathrm{Re}[\mathcal{F}_S(\epsilon)]\mathrm{Im}[\mathcal{F}_{S'}(\epsilon)]\}\right|, \quad (1)$$

where $\mathcal{F}_{S,S'}(\epsilon) = \Delta_{S,S'}/\sqrt{(\epsilon + i\Gamma_{S,S'})^2 - \Delta^2_{S,S'}}$. In the above expressions we set $\Delta_S = \Delta_S(T_{\mathrm{bath}})$ and $\Delta_{S'} = \Delta_{S'}(T'_e)$. Equation (1) shows that I_J is controlled by T'_e once T_{bath} is fixed. Under bias voltage V_{inj} the heat current ($\dot{Q}_{L,R}$) flowing from S' to S through L or R interface is given by [17,21]

$$\dot{Q}_{L,R} = \frac{1}{e^2R_T}\int d\epsilon\bar{\epsilon}\mathcal{N}_S(\tilde{\epsilon}_{L,R})\mathcal{N}_{S'}(\bar{\epsilon})[f_0(\bar{\epsilon},T'_e) - f_0(\tilde{\epsilon}_{L,R},T_{\mathrm{bath}})]. \quad (2)$$

T'_e is then determined by solving the energy-balance equation $\dot{Q}_L(V_{\mathrm{inj}},T_{\mathrm{bath}},T'_e) + \dot{Q}_R(V_{\mathrm{inj}},T_{\mathrm{bath}},T'_e) = 0$. We neglect the electron-phonon interaction contribution in the energy-balance equation which would lead to small corrections only. The probe supercurrent is then determined by the electron temperature T'_e established in S' by biasing the control line.

For comparison with the experiment we chose the given parameters of Sample B, $T_c = 1.2$ K and depairing parameter $\Gamma_{S(S')} = 5\times10^{-3}\Delta_{S(S')}$. The injector current-voltage characteristics calculated at different T_{bath} are displayed on the right axis of Fig. 4(b). In addition to Josephson coupling vanishing at $T_{\mathrm{bath}} \geq T'_c$, the current shows a peak centered in the middle of the characteristic, as observed in the experiment [see right axis of Figs. 3(a) and 3(b)]. The I_J vs V_{inj} characteristics are displayed on the left axis of Fig. 4(b) for the same T_{bath} values. The supercurrent curves of Figs. 3(a) and 3(b) resemble those of the model presented in Fig. 4(a), apart from details that we attribute to the oversimplified thermal model.

Figure 4(c) shows the electron temperature T'_e calculated from the energy-balance equation for the corresponding bath temperatures. For $T_{\mathrm{bath}} \leq 200$ mK the electron gas is initially heated, inducing supercurrent suppression at small bias voltages. Such heating stems from subgap current in a tunnel junction [2,22,23]. By increasing V_{inj} further, the electron temperature starts to decrease, thanks to quasiparticle cooling [2,21] provided by the larger gap superconductor (S), and is minimized at $V_{\mathrm{inj}} \simeq 150\ \mu$V. Further increase of bias voltage leads again initially to heating, then cooling, and eventually heating above T'_c for large V_{inj}. At the bath temperature of 250 mK, T'_e starts to decrease monotonically, initially driving S' into the superconducting state, and showing the same behavior as at lower T_{bath}.

In conclusion, control of Josephson current as well as its generation at bath temperatures above the critical one were achieved by varying quasiparticle injection into a small superconducting island. Our results are successfully described within a model relating the superconducting state of the island to the heat flux originating from quasiparticle injection. From the practical point of view, our experiment demonstrates that quasiparticle injection can cool a metal wire from its normal state deep into the superconducting phase.

We acknowledge financial support from the EU Large Scale Installation Program ULTI-3 and from the NanoSciERA "NanoFridge" project.

*giazotto@sns.it

[1] N. B. Kopnin, *Theory of Nonequilibrium Superconductivity* (Clarendon Press, Oxford, 2001).
[2] F. Giazotto *et al.*, Rev. Mod. Phys. **78**, 217 (2006).
[3] F. K. Wilhelm, G. Schön, and A. D. Zaikin, Phys. Rev. Lett. **81**, 1682 (1998).
[4] A. F. Volkov, Phys. Rev. Lett. **74**, 4730 (1995).
[5] F. Giazotto *et al.*, Phys. Rev. Lett. **92**, 137001 (2004).
[6] J. J. A. Baselmans *et al.*, Nature (London) **397**, 43 (1999).
[7] A. M. Savin *et al.*, Appl. Phys. Lett. **84**, 4179 (2004).
[8] A. F. Morpurgo, T. M. Klapwijk, and B. J. van Wees, Appl. Phys. Lett. **72**, 966 (1998).
[9] M. S. Crosser *et al.*, Phys. Rev. Lett. **96**, 167004 (2006).
[10] F. Giazotto and J. P. Pekola, J. Appl. Phys. **97**, 023908 (2005).
[11] M. A. Laakso *et al.*, Phys. Rev. B **75**, 094507 (2007).
[12] M. G. Blamire *et al.*, Phys. Rev. Lett. **66**, 220 (1991).
[13] G. Ammendola *et al.*, IEEE Trans. Appl. Supercond. **9**, 3974 (1999).
[14] A. Brinkman *et al.*, IEEE Trans. Appl. Supercond. **11**, 1146 (2001).
[15] I. P. Nevirkovets, Phys. Rev. B **56**, 832 (1997).
[16] I. P. Nevirkovets, O. Chernyashevskyy, and J. B. Ketterson, Phys. Rev. B **73**, 224521 (2006).
[17] A. J. Manninen *et al.*, Appl. Phys. Lett. **74**, 3020 (1999).
[18] V. Ambegaokar and A. Baratoff, Phys. Rev. Lett. **10**, 486 (1963); **11**, 104(E) (1963).
[19] A. Steinbach *et al.*, Phys. Rev. Lett. **87**, 137003 (2001).
[20] Yu. M. Ivanchenko and L. A. Zil'berman, Sov. Phys. JETP **28**, 1272 (1969).
[21] B. Frank and W. Krech, Phys. Lett. A **235**, 281 (1997).
[22] J. P. Pekola *et al.*, Phys. Rev. Lett. **92**, 056804 (2004).
[23] S. Rajauria *et al.*, Phys. Rev. Lett. **100**, 207002 (2008).